Available online at www.sciencedirect.com
ScienceDirect
Trans. Nonferrous Met. Soc. China 26(2016) 3059−3069
Transactions of Nonferrous Metals Society of China
www.tnmsc.cn

Grain refinement mechanism of as-cast aluminum by hafnium

Hong-ying LI[1], De-wang LI[1], Zhi-xiang ZHU[2,3], Bao-an CHEN[2,3], Xin CHEN[2,3], Chang-long YANG[4], Hong-yu ZHANG[4], Wei KANG[1]

1. School of Materials Science and Engineering, Central South University, Changsha 410083, China;
2. New Electrical Materials and Microelectronics Department, Global Energy Interconnection Research Institute, Beijing 102211, China;
3. State Key Lab of Advanced Power Transmission Technology, Beijing 102211, China;
4. State Grid Liaoning Electric Power Supply Co., Ltd., Shenyang 110006, China

Received 11 November 2015; accepted 26 April 2016

Abstract: The effect of Hf on the grain refinement of as-cast aluminum was investigated using optical microscopy, electron microscopy and X-ray diffraction. The result shows that the grain size of studied alloy decreases effectively with the addition of Hf, Hf can react with Al to form Al_3Hf particles during the solidification, the primary Al_3Hf particles are highly potent nucleants for Al and the nanoscale coherent Al_3Hf particles can inhibit the grain growth by pinning effect. The grain refinement mechanism of studied alloys was verified by the solute theory and the crystallography study, and it can be divided into two distinct types: At low Hf contents, there are no primary Al_3Hf phases to form, the acquired grain refinement is primarily attributed to the constitutional undercooling induced by the Hf solute. At medium and high Hf contents, both Hf solute and Al_3Hf particles contribute to the refinement.

Key words: grain refinement mechanism; aluminum alloy; casting; Hf; Al_3Hf

1 Introduction

Aluminum and its alloys are attractive engineering materials for structural applications in many industries, because of the low density and good electrical conductivity, good resistance to corrosion, excellent thermal conductivity [1]. The properties of aluminum alloys are governed by many microstructural features including the grain size. Grain refinement of Al alloys is a predominant technique to control the metallurgical characteristics and to improve the soundness of cast alloys, which has been extensively investigated by many researchers for over 80 years [2−5]. It can get a fine equiaxed grain structure of α(Al) through grain refinement, which can eliminate the columnar structure, ensure uniform mechanical properties, improve formability and machinability, reduce casting defects and tearing tendency as well as enhance subsequent mechanical working response [6−11]. Grain refinement also has a significant impact on the aluminum conductors: a fine grain will give rise to high tensile strength based on the fine-grained strengthening theory, but it will increase grain boundary and therefore result in the decrease of electrical conductivity. Thus, it is important to study the mechanism of grain refinement in aluminum conductors.

Several methods have been reported to achieve grain refinement in the final microstructure, such as inoculation, heterogeneous nucleation, solute addition, mechanical agitation [3,10,12,13]. The addition of transition metals or rare earth metals, such as Sc and Zr, can refine the grain of as-cast Al alloys effectively [3,4,6,14]. This is because Zr or Sc can result in the formation of primary Al_3Sc or Al_3Zr phases as well as nanoscale coherent $L1_2$ structured Al_3Sc or Al_3Zr particles, which can behave as potent nucleant particles for Al or inhibit the migration of grain boundary or subboundary, thus will lead to the grain refinement [4,15−17]. The mechanisms of the grain refinement such as the solute theory (the growth restriction factor concept and the relative grain size concept) and the heterogeneous nucleation theory (the crystallographic using the edge-to-edge matching model) have been reported in

Foundation item: Project (SGRI-WD-71-13-001) supported by the Scientific and Technological Project of State Grid Corporation of China
Corresponding author: Hong-ying LI; Tel: +86-731-88836328; E-mail: lhying@csu.edu.cn
DOI: 10.1016/S1003-6326(16)64438-2

many literatures [3,6,18−24]. It is widely believed that both effective nucleation particles and abundant solutes are indispensable for efficient grain refinement [6,25−28].

Similar to Sc or Zr, Hf can form the nanoscale coherent $L1_2$ structured Al_3Hf precipitate in Al matrix, which has been studied by WU et al [29]. However, up to now, few researches have been investigated in the published literatures about the grain refinement mechanism of as-cast alumnium by hafnium. In the present study, Al−Hf alloys with different Hf addition levels were prepared through conventional casting processes, the grain refinement mechanism was revealed and it can provide experimental evidence to understand the grain refining mechanism in cast metals through inoculation treatment.

2 Experimental

The experimental alloys with different Hf addition levels (0.1%, 0.15%, 0.2%, 0.3%, 0.4%, 0.5% and 0.6%, mass fraction) were prepared by diluting commercially pure aluminum with Al−10.45Hf master alloys (mass fraction, %). The raw materials were melted in a graphite crucible in a resistively heated furnace at 750 °C, after mechanical stirring the melt was cast into an iron water-cooled mould and cooled to room temperature to produce a *d*50 mm × 100 mm ingots. The chemical compositions of the investigated alloys were verified using ICP−MS analysis and listed in Table 1 (all compositions were in mass fraction unless otherwise noted).

Table 1 Compositions of experimental alloys (mass fraction, %)

Sample	Hf	Fe	Si	Cu	Mg	Al
Pure Al	0.001	0.021	0.0085	0.0032	0.0092	Bal.
Al−0.1Hf	0.09	0.047	0.011	0.0037	0.011	Bal.
Al−0.15Hf	0.16	0.034	0.013	0.0062	0.017	Bal.
Al−0.2Hf	0.21	0.022	0.014	0.0091	0.015	Bal.
Al−0.3Hf	0.29	0.048	0.010	0.0058	0.012	Bal.
Al−0.4Hf	0.38	0.025	0.017	0.0085	0.019	Bal.
Al−0.5Hf	0.47	0.041	0.008	0.0046	0.010	Bal.
Al−0.6Hf	0.59	0.062	0.007	0.0074	0.0099	Bal.

Approximately 10 mm sized metallographic specimens were taken from the cast ingots and were mechanically ground, polished by grit paper and then etched by a solution of 1 mL HF, 1.5 mL HCl, 2.5 mL HNO_3 and 95 mL distilled water. After sample preparation, the metallographic structures were characterized by optical microscopy (OM) and using the IPP (Image Pro-Plus) soft to measure the grain sizes. Phase identification was conducted by X-ray diffraction analysis in a SI-MENSD500 full-automatic X-ray diffractometer, operating at 40 kV and 45 A with Cu K_α radiation. Transmission electron microscope (TEM) and scanning electron microscope (SEM) observations were performed with a FEI Tecnai G^220 operated at 200 kV and FEI Quanta-200, respectively. TEM samples were prepared by mechanical grinding specimens to a thickness of 80−100 μm, from which 3 mm diameter disks were punched. The disks were then thinned by twin-jet electro-polishing at ~20 V DC with an electrolyte solution consisting of 30% nitric acid and 70% methanol below −30 °C.

3 Results and discussion

3.1 Macrostructure and microstructure of as-cast aluminum alloys

Figure 1 shows the macrographs of as-cast aluminum grain refined with 0.1%, 0.15%, 0.2%, 0.3%, 0.4%, 0.5% and 0.6% addition level of Hf element, respectively. As illustrated in Fig. 1(a), in the absence of Hf, the aluminum manifests a mixture of complete coarse columnar grain structure at the periphery and coarse equiaxed grains at the center. After adding 0.1% Hf into pure aluminum, the average size of coarse columnar grains and equiaxed grains decrease, as shown in Fig. 1(b). Having a comparison among Figs. 1(c), (d) and (e), it is noted that the columnar grains change to equiaxed grains with the increase of Hf content, and the average grain size is also decreased. When the addition increases to 0.4%, as seen in Fig. 1(f), only fine equiaxed grains are observed. But further increasing the addition level of Hf, equiaxed grain size do not further decrease, as shown in Figs. 1(g) and (h).

The optical microstructures of the as-cast aluminum with different Hf contents are presented in Fig. 2. It can be obviously seen that the grains can be refined dramatically by adding Hf element. Without Hf addition, the average grain size is around 440 μm, with the increasing additions of Hf content from 0.1% to 0.3%, the average grain size decreases continuously from 434 to 251 μm. When 0.4% Hf is added, the average grain size reaches 219 μm, but further increasing the Hf contents from 0.4% to 0.6%, there is no significant improvement in the grain refinement. The smallest grains with the grain size of 196 μm are obtained when the addition reaches 0.6%.

3.2 Determination of relative grain size

The mechanisms of grain refinement such as the solute effect and the heterogeneous nucleation effect

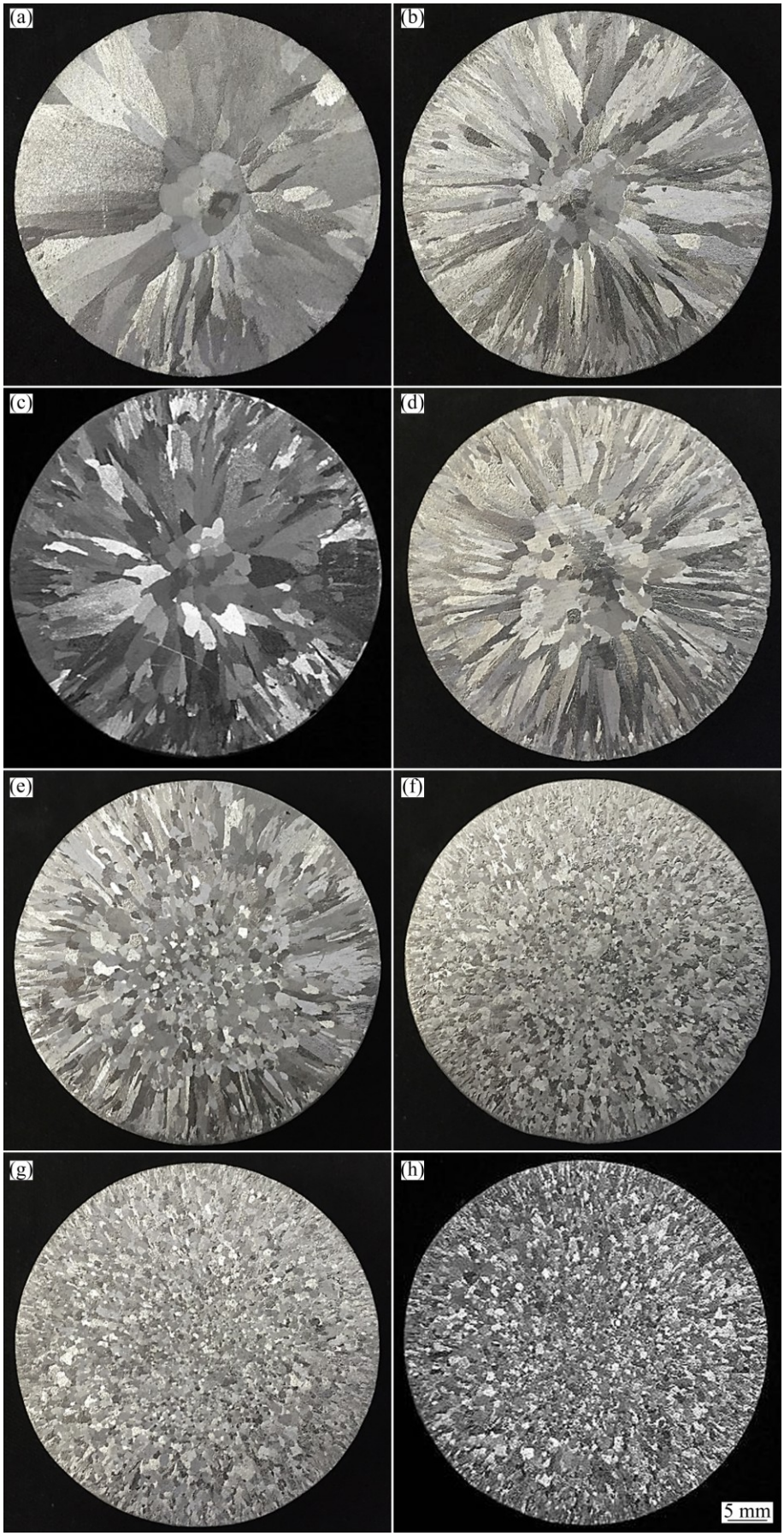

Fig. 1 Macrographs of as-cast experimental aluminum alloys: (a) Pure aluminum; (b) Al−0.1Hf; (c) Al−0.15Hf; (d) Al−0.2Hf; (e) Al−0.3Hf; (f) Al−0.4Hf; (g) Al−0.5Hf; (h) Al−0.6Hf

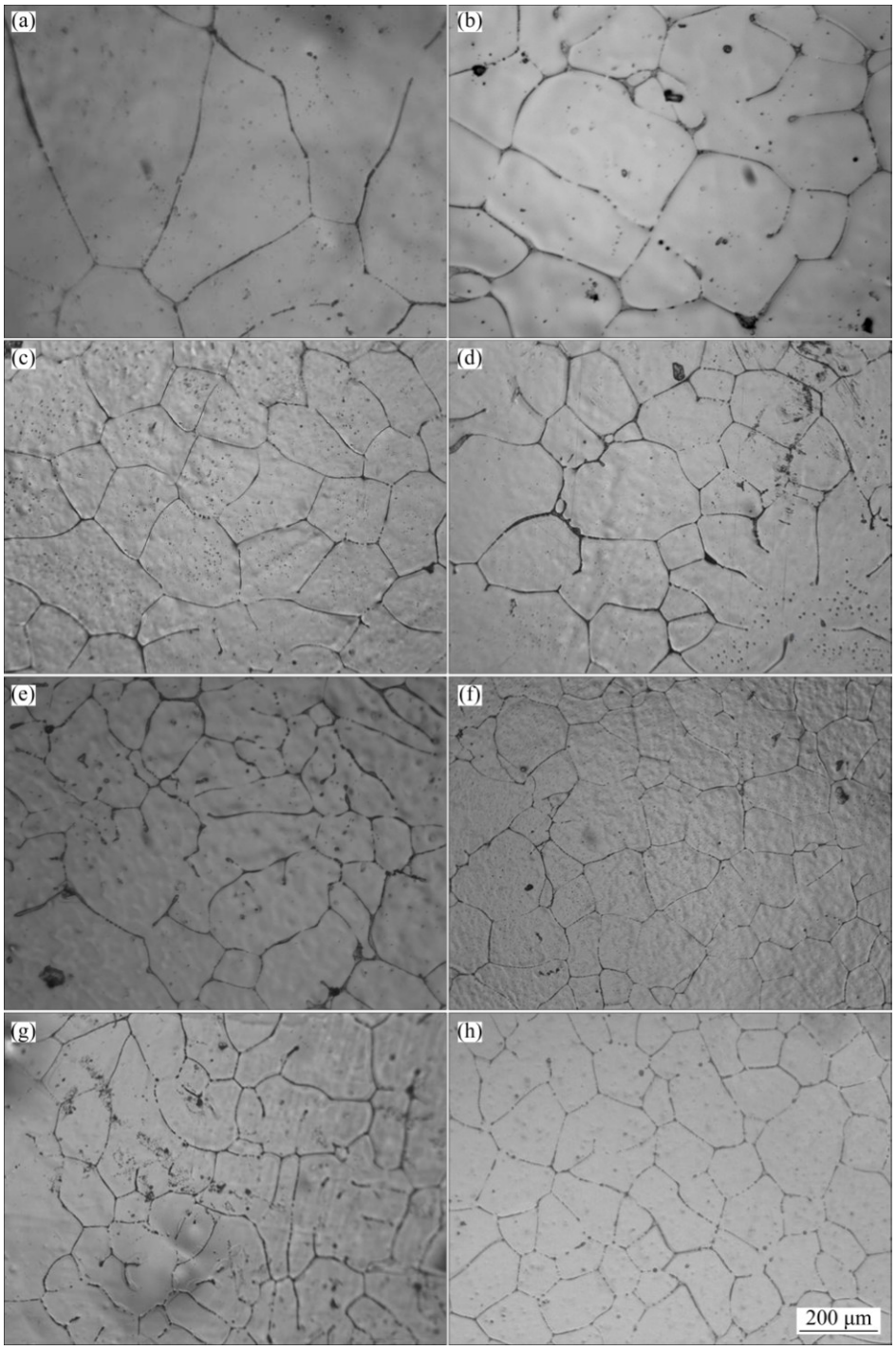

Fig. 2 Micrographs of as-cast experimental aluminum alloys: (a) Pure aluminum; (b) Al−0.1Hf; (c) Al−0.15Hf; (d) Al−0.2Hf; (e) Al−0.3Hf; (f) Al−0.4Hf; (g) Al−0.5Hf; (h) Al−0.6Hf

have been reported in literatures [6,18−20]. STJOHN et al [18,19] reported that the growth restriction factor (GRF), Q, can be used to quantify the effect of solute on the grain size of a casting alloy. It is generally accepted that the high value of Q is desirable to refine the grain in alloys [18−20,30,31]. The value of Q can be calculated by $m_1c_0(k-1)$, where m_1 is the slope of the liquidus line on the binary phase diagram, c_0 is the concentration of the solute in a binary alloy and k is the partition coefficient.

The calculated Q value of Hf alloyed to aluminum equals $11.2c_0$ (c_0 is the concentration), which is in the upper level among the most common alloying elements used in Al alloys when c_0 remains the same [25,32]. Thus, it is easy to consider that the solute effect of Hf makes major contribution to the grain refinement of the as-cast aluminum. However, STJOHN et al [18,19] found that only when powerful nucleants are presented

can the Q value be used to predict the effect of solute content on grain size accurately. Therefore, a new concept, relative grain size (RGS), was put forward to explain the relationship between grain size and the combined effects of nucleant particle potency and solute content, which is given by

$$\mathrm{RGS}=1-\left(\frac{m_1c_0}{m_1c_0-\Delta T_n}\right)^{\frac{1}{p}} \tag{1}$$

where m_1 is the slope of the liquidus line, c_0 is the composition of the alloy, p equals $1-k$, where k is the partition coefficient, and ΔT_n is the nucleant particle potency or the undercooling required for nucleation.

Curves (a)−(f) of Fig. 3 present the RGS of the studied alloy versus Hf solute content at different nucleant particle potencies, ΔT_n. It can be seen that particle potency ΔT_n has a remarkable influence on Al grain size for all solute contents, while the effect of Hf solute content on grain size is conspicuous at low content and inconspicuous at high content and as ΔT_n increases the effect will be remarkably weakened. The variation of the average grain size as a function with the Hf addition level in Fig. 2 is shown by curve (g) of Fig. 3, it is found that the change of the grain size in this work (curve g) is similar to the trend predicted by RGS when the ΔT_n is equal to 0.01 °C (curve d). Because the ΔT_n represents the undercooling required for nucleation, it is apparent that only when the constitutional undercooling, ΔT_c, reaches ΔT_n can a nucleation event occur. The ΔT_c is defined by

$$\Delta T_c=m_1c_0\left(1-\frac{1}{(1-f_s)^p}\right) \tag{2}$$

where f_s is the solid fraction.

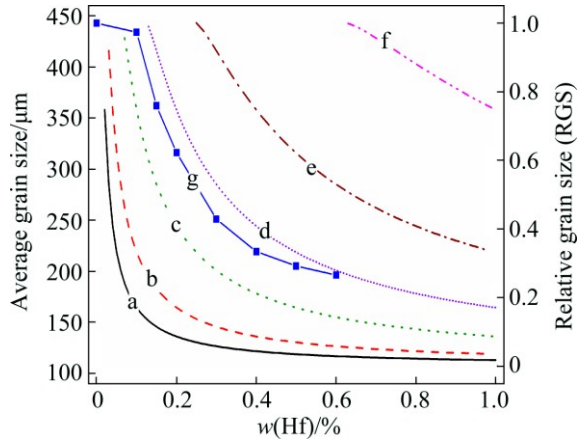

Fig. 3 RGS vs solute content for range of nucleant particle potencies ΔT_n: (a) ΔT_n=0.001 °C; (b) ΔT_n=0.002 °C; (c) ΔT_n=0.005 °C; (d) ΔT_n=0.01 °C; (e) ΔT_n=0.02 °C; (f) ΔT_n=0.05 °C and average grain size variation of experimental alloys (g)

The development of constitutional undercooling versus solid fraction for different additions of Hf, calculated using Eq. (2), is shown in Fig. 4. It is observed that the constitutional undercooling increases with the increasing additions of Hf content and the increase amplitude is obvious. Therefore, a relative decrease in the grain size as the Hf level increases would be expected, which is consistent with the experimental result. Equations (1) and (2) are all based on the assumption that there are sufficient nucleant particles or substrates present in the matrix, namely there should be potential nucleation sites for the metal matrix during solidification process [18−20,30,31]. In industrial practice, inoculation whose lattice structure and lattice constant should match up with the master alloy is often used to promote nucleation [5,11,28,33], in this process, there will be many potential nucleation sites to be formed.

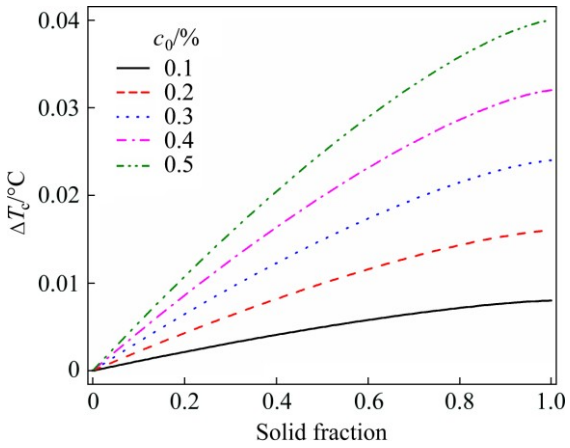

Fig. 4 Development of constitutional undercooling, ΔT_c, versus solid fraction for different additions of Hf

3.3 Crystallographic relationship between Al_3Hf and Al matrix

To better investigate the grain refinement mechanism, phase identification was conducted by XRD analysis and the corresponding XRD patterns of the as-cast alloy sample without Hf addition and with 0.4% Hf addition are shown in Figs. 5(a) and (b) , respectively. It can be seen that Fig. 5(a) exhibits a typical XRD spectrum of α(Al), and no precipitates or intermetallic compounds are observed. While weak Al_3Hf peaks can be observed in Fig. 5(b), which indicates that a small quantity of Al_3Hf particles precipitate in the matrix. WANG et al [21,24] found that Al_3Zr and Al_3Nb are potent heterogeneous nucleation refiners for Al grains by means of the edge-to-edge matching (E2EM) model. Al_3Hf possesses the similar crystal structure characterization with Al_3Zr or Al_3Nb. Thus, it can be speculated that the Al_3Hf particles may be the potential nucleation sites and the E2EM model is employed to

confirm this extrapolate.

The E2EM model developed by ZHANG et al [3,21−24] is a powerful tool in understanding and examining the atomic matching between the nucleant phase and matrix which has been applied widely in illuminating the grain refinement mechanism. The model requires that the matching rows (termed matching directions) should be close-packed (CP) or nearly CP atom rows with small interatomic spacing misfit (f_r) and lie on the CP or nearly CP planes (termed matching planes) with interplanar spacing mismatch (f_d). The matching rows can be either straight or zigzag, but the model requires that straight rows match with straight rows while zigzag rows match with zigzag rows. Once the f_r of the matching direction and the f_d of the matching planes are smaller than 10%, an orientation relationships (OR) can potentially form and can be expressed in terms of the parallelism of the matching rows and near parallelism of the matching planes.

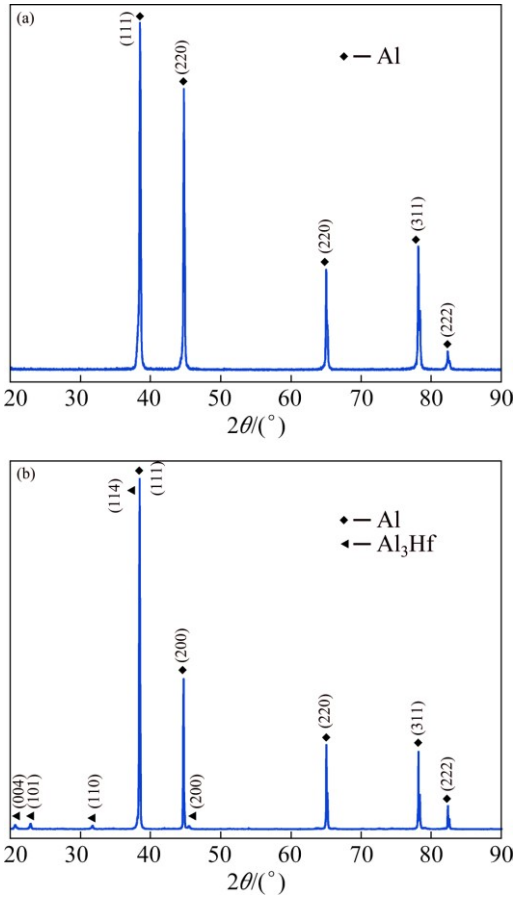

Fig. 5 XRD patterns of as-cast aluminum alloys: (a) Without addition of Hf; (b) 0.4% Hf addition

According to the knowledge of crystallography, aluminum has face-centred cubic (FCC) structure, its lattice constant A is equal to 0.4049 nm. It has two possible CP or nearly CP atom rows: $\langle 110\rangle^{S}_{Al}$ and $\langle 211\rangle^{Z}_{Al}$, where the superscript "S" denotes straight atom rows and "Z" indicates the zigzag atom rows. The possible CP or nearly CP planes of Al are: $\{200\}_{Al}$, $\{220\}_{Al}$, $\{111\}_{Al}$. The $\{111\}_{Al}$ plane belongs to CP planes, which includes both the $\langle 110\rangle^{S}_{Al}$ and $\langle 211\rangle^{Z}_{Al}$ directions. The second most highly CP plane is $\{200\}_{Al}$, which only includes the $\langle 110\rangle^{S}_{Al}$ direction. The $\{220\}_{Al}$ plane is the third CP plane, in $\{220\}_{Al}$ plane $\langle 110\rangle^{S}_{Al}$ and $\langle 211\rangle^{Z}_{Al}$ CP directions exist. The atomic configuration of Al within the most highly CP plane (111) is displayed in Fig. 6(a).

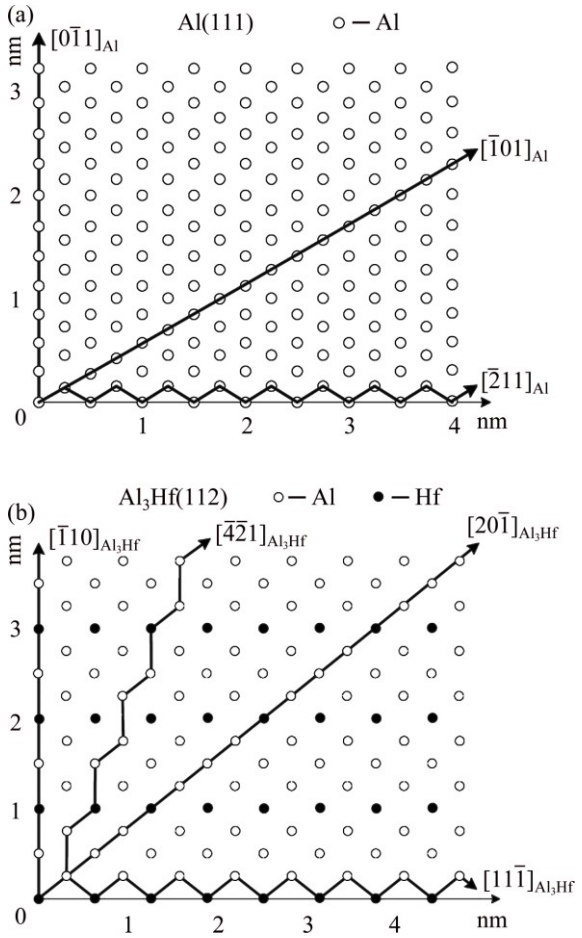

Fig. 6 Atomic configurations of Al (a) and Al_3Hf (b) on their most highly CP planes (Bold lines highlight the CP rows within these planes)

Al_3Hf possesses three CP or nearly CP planes, they are $\{112\}_{Al_3Hf}$, $\{004\}_{Al_3Hf}$ and $\{200\}_{Al_3Hf}$. The most highly CP plane $\{112\}_{Al_3Hf}$ contains four CP or nearly CP rows: $\langle 421\rangle^{Z}_{Al_3Hf}$, $\langle 111\rangle^{Z}_{Al_3Hf}$, $\langle 110\rangle^{S}_{Al_3Hf}$, and $\langle 201\rangle^{S}_{Al_3Hf}$; the second most highly CP plane is $\{004\}_{Al_3Hf}$, which contains only $\langle 110\rangle^{S}_{Al_3Hf}$ CP row; $\{200\}_{Al_3Hf}$ is another possible CP plane which also contains one CP row $\langle 201\rangle^{S}_{Al_3Hf}$. The atomic configuration of Al_3Hf within the most highly CP plane (112) is displayed in Fig. 6(b).

Table 2 lists the values of f_r along the CP rows between Al_3Hf and Al by following the E2EM model

matching rules. It can be seen that all the values of f_r are less than 6%. The calculated f_d between Al_3Hf and Al CP planes are listed in Table 3. It is obviously that only four pairs of planes with f_d below 10% exist: $\{111\}_{Al}//\{112\}_{Al_3Hf}$ with f_d=0.89%, $\{200\}_{Al}//\{200\}_{Al_3Hf}$ with f_d=3.07%, $\{111\}_{Al}//\{004\}_{Al_3Hf}$ with f_d=5.19%, $\{200\}_{Al}//\{004\}_{Al_3Hf}$ with f_d=9.47%.

Table 2 Interatomic spacing misfit, f_r, along CP matching rows between Al_3Hf and Al

Matching row	f_r/%
$\langle 110\rangle^{S}_{Al}//\langle 110\rangle^{S}_{Al_3Hf}$	3.08
$\langle 110\rangle^{S}_{Al}//\langle 201\rangle^{S}_{Al_3Hf}$	3.48
$\langle 211\rangle^{Z}_{Al}//\langle 111\rangle^{Z}_{Al_3Hf}$	5.58
$\langle 211\rangle^{Z}_{Al}//\langle 421\rangle^{Z}_{Al_3Hf}$	0.84

Table 3 Interplanar spacing mismatch, f_d, between CP or nearly CP planes in Al_3Hf and Al

Matching plane	f_d/%
$\{200\}_{Al}//\{004\}_{Al_3Hf}$	9.47
$\{200\}_{Al}//\{200\}_{Al_3Hf}$	3.07
$\{200\}_{Al}//\{112\}_{Al_3Hf}$	16.50
$\{220\}_{Al}//\{004\}_{Al_3Hf}$	54.82
$\{220\}_{Al}//\{200\}_{Al_3Hf}$	37.08
$\{220\}_{Al}//\{112\}_{Al_3Hf}$	64.76
$\{111\}_{Al}//\{004\}_{Al_3Hf}$	5.19
$\{111\}_{Al}//\{200\}_{Al_3Hf}$	16.06
$\{111\}_{Al}//\{112\}_{Al_3Hf}$	0.89

Figure 7 graphically shows the values of f_r that are below 10% along the matching directions (on left) and the values of f_d that are less than 10% between matching planes that contain the matching directions (on right). The arrows are used to point out the correlation between a matching direction pair with various matching plane pairs. From Fig. 7, it can be clearly seen that seven ORs between Al and Al_3Hf can potentially form and possibly be observed, which implies high inoculation potency of Al_3Hf particles for α(Al).

Figure 8(a) shows the SEM image of the sample used to obtain the XRD spectrum as shown in Fig. 4(b). It is found that, when 0.4% Hf is added, small particles can be observed at or near the centers of the grains, as shown by particle A and particle B in Fig. 8(a). These particles are believed to act as heterogeneous nucleation sites during solidification [24]. Figure 8(b) shows a typical EDX spectrum of particle *A* in Fig. 8(a), it is shown that the particle is rich in Al and Hf and the approximate atomic ratio of Al to Hf is about 3:1. Considering the XRD and EDX results, it is confirmed that the particles observed at or near the grain centers are Al_3Hf particles. Hence, based on the crystallographic analysis using the E2EM model, the SEM observations and the EDX analysis, the potency of Al_3Hf particles as nucleation sites for Al grains can be evaluated.

3.4 Grain refinement mechanism

Based on the preceding study, it can be concluded that both the Hf solute and the Al_3Hf particle have effect on the grain refinement of Al. To better understand the effect of solute and the effect of nuclei on grain size of Al, the grain size can be expressed as Eq. (3) [19,25,26,32,34−36].

$$d = a + \frac{b}{Q} \tag{3}$$

where d is the grain size, the slope b corresponds to the potency of the nucleant particles which is related to the solute, the intercept a corresponds to the number of particles which is related to the activated nuclei. The slope b and the intercept a will decrease with the increase of the potency of the nuclei and the number of nuclei, respectively.

Replotting the measured grain size data in current work against $1/Q$ gives Fig. 9, it can be seen that the trend-line of grain size vs $1/Q$ cannot be fitted through a

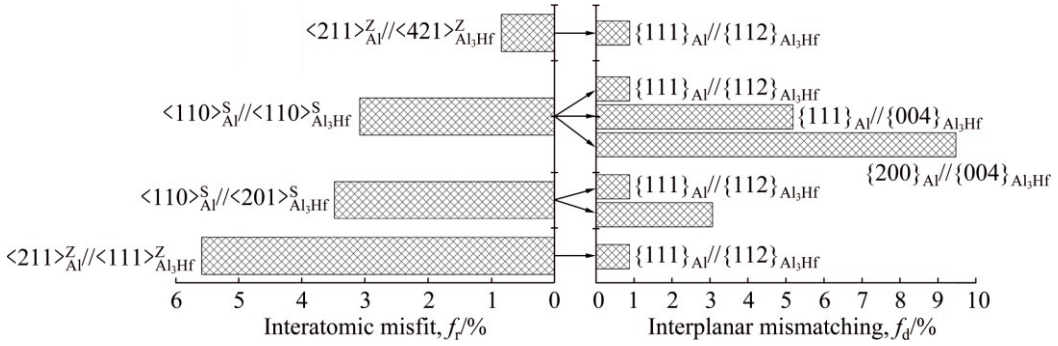

Fig. 7 Graphic representation of matching row pairs (Table 1) and related suitable matching plane pairs (Table 2) which carry them, as predicted by E2EM model

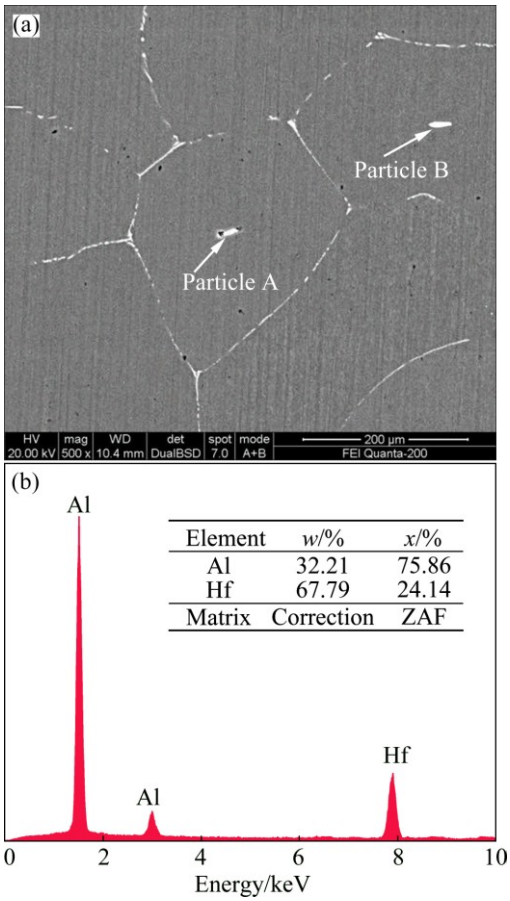

Fig. 8 SEM image of as-cast experimental alloy with addition of 0.4% Hf (a) and EDX spectrum taken from particle A in Fig. 8(a) (b)

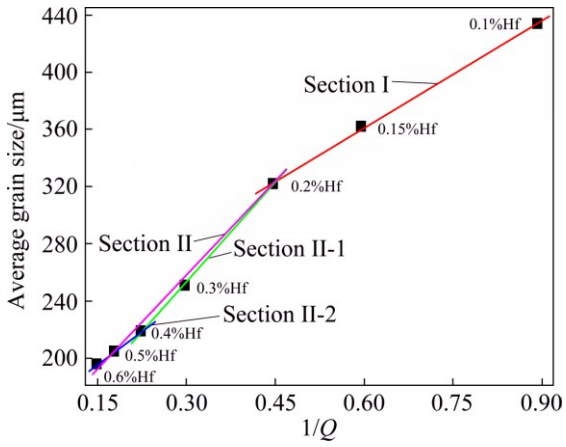

Fig. 9 Grain size of as-cast aluminum alloys with different additions of Hf plotted against growth restriction factor $1/Q$

single line, but can be fitted by two separate lines. According to different meanings of a and b in Eq. (3), the process of grain refinement with the increasing of Hf addition can be divided into two sections, as shown in Fig. 9, and each section possesses different types of grain refinement mechanism. The Al-rich portion of the Al−Hf phase diagram is shown in Fig. 10. It can be seen that the maximum hafnium solubility in liquid aluminum at the peritectic temperature is 0.43%. Therefore, when the content of Hf is below 0.43%, there will be no primary Al_3Hf phase to form and the peritectic reaction could not happen in equilibrium solidification, thus the Hf addition cannot refine Al grain through heterogeneous nucleation. But because of the non-equilibrium solidification and the effect of impurities, the threshold of 0.43% will decrease.

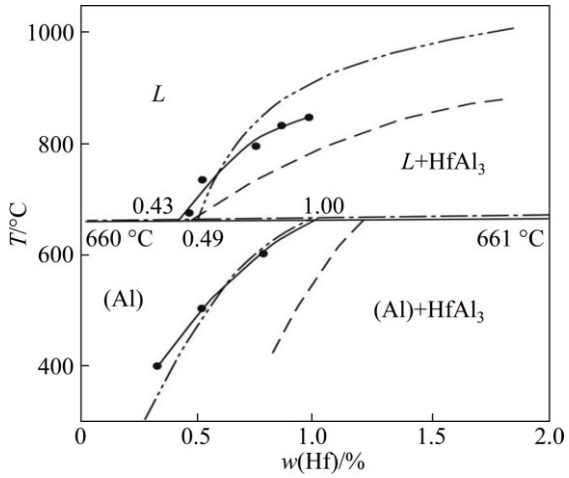

Fig. 10 Al-rich portion of Al−Hf phase diagram [37,38]

Table 4 lists the values of the intercept a and gradient b of the two sections after linear fitting, it can be seen that section I has higher value a and lower numerical b. According to the different meanings of a, b and combining with the phase diagram, it can draw a conclusion that because of the low addition of Hf element, the alloy shows low potency nucleant particles and there will be no primary Al_3Hf particle to be formed, thus the grain refinement is primarily through the contribution of the solute segregation in section I.

Table 4 Values of intercept a and gradient b of grain size vs $1/Q$ lines presented in Fig. 9

Section	Intercept a	Gradient b	R^2
I	211.71	249.60	0.9986
II	127.68	428.37	0.9914

*R^2 is the correlation coefficient.

When the adding amount exceeds 0.2%, the intercept a reduces and the gradient b increases, then the process of grain refinement enters section II. In this section, because of the large adding amount of Hf element as well as the non-equilibrium solidification and the effect of impurities, a significant number of Al_3Hf nucleant particles are introduced into the melt, which could increase the population of active nuclei in the melt and therefore cause obvious grain refinement through

heterogeneous nucleation. But in section II, the gradient *b* does not increase to infinity, it just increases about 70% in comparison to the gradient *b* of section I, so in this section the constitutional undercooling still has influence on the grain refinement. Thus, in section II, both constitutional undercooling and heterogeneous nucleation contribute to the grain refinement.

A small and stable grain size is usually achieved by using materials containing precipitates which serve to impede grain boundary mobility and thereby restrict the development of grain growth [39]. It is found that through alloying treatment, Zr or Sc can result in the formation of Al_3Sc or Al_3Zr particles in the Al matrix during the solidification [40], these nanoscale coherent $L1_2$ structured particles can stabilize the grain structure by inhibiting the migration of grain and subgrain boundaries through pinning effect [4,15−17]. Similar to the Sc or Zr, Hf element can also react with Al element to form the nanoscale coherent $L1_2$ structured Al_3Hf precipitate during the freezing of cast, which has been proved by the TEM images of the as-cast aluminum alloys in Figs. 11(a) and (c). It is observed that when 0.4% Hf was added, many fine and dispersive Al_3Hf phases which are coherent with the Al matrix (determined from the Ashby−Brown strain-field contrast) precipitated homogeneously in alloy, and these precipitates can prevent the grain boundary migration by means of pinning effect, as shown by Fig. 11(b).

The grain refinement process in section II includes two stages, II-1 and II-2, as shown by Fig. 9. In section II-1, the Hf content is below 0.5%, the grain refinement effect is remarkable, which attributes to the solute segregation and the heterogeneous nucleation as well as the pinning effect by the nanoscale coherent $L1_2$ structured Al_3Hf precipitates. When Hf content increases up to 0.5%, it moves into the second stage. By contrast with section II-1, the grain refinement effect of Hf on Al weakens in section II-2. This may be because that the tendency of coarsening for Al_3Hf particles will rapidly increase due to the large adding amount of Hf element, and the number density of the total Al_3Hf particles will decline drastically, which can be verified by comparing Figs. 11(a) and (d). In the meantime, quite a few Al_3Hf particles lose the coherent with the matrix, as shown in

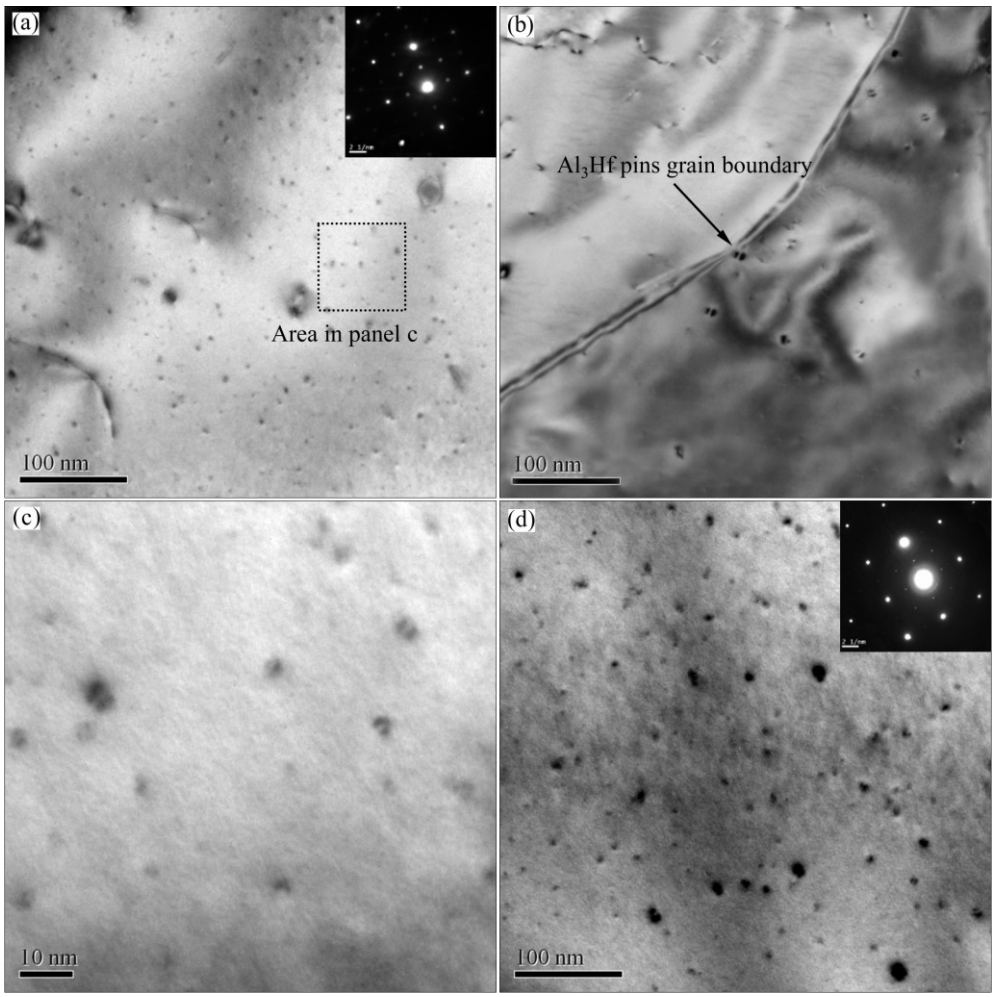

Fig. 11 TEM images of as-cast aluminum alloys: (a) and (b) Bright-field image of Al−0.4Hf; (c) Magnified view of Al_3Hf; (d) Bright-field image of Al−0.5Hf

Fig. 11(d), and cannot stabilize the grain structure by impeding grain boundary mobility and thereby cannot restrict the development of grain growth.

4 Conclusions

1) The grain size of studied alloy decreases effectively with the increasing of Hf content. Increasing the content of Hf from 0 to 0.6%, the grain size reduces from 443 to 196 μm. The Hf element can react with Al to form Al_3Hf intermetallic compound during the solidification.

2) The effect of Hf solute content on grain size is conspicuous at low content and inconspicuous at high content. The E2EM model indicates that the interatomic spacing misfit and interplanar mismatch between Al_3Hf and Al are very small, implying that the Al_3Hf particles are highly potent nucleants for Al.

3) The grain refinement mechanism possesses two types with the increasing of Hf addition. At low Hf contents, there are no primary Al_3Hf phases to form in the melt, the acquired grain refinement is mainly due to the constitutional undercooling induced by the Hf solute. At medium and high Hf contents, both Hf solute and Al_3Hf particles contribute to the refinement.

Acknowledgments

This research is supported by Scientific and Technological Project of State Grid Corporation of China (No. SGRI-WD-71-13-001). The authors wish to express gratitude to Pro. Ming-xing ZHANG of the University of Queensland for providing important literatures.

References

[1] NOWAK M, BOLZONI L, HARI BABU N. Grain refinement of Al−Si alloys by Nb−B inoculation. Part I: Concept development and effect on binary alloys [J]. Materials & Design, 2015, 66(Part A): 366−375.

[2] ZHANG Yi-jie, MA Nai-heng, YI Hong-zhan, LI Song-chun, WANG Hao-wei. Effect of Fe on grain refinement of commercial purity aluminum [J]. Materials & Design, 2006, 27(9): 794−798.

[3] ZHANG M X, KELLY P M, EASTON M A, TAYLOR J A. Crystallographic study of grain refinement in aluminum alloys using the edge-to-edge matching model [J]. Acta Materialia, 2005, 53(5): 1427−1438.

[4] GAO Zhao-he, LI Hong-ying, LAI Yong-qiu, OU Yang-xun, LI De-wang. Effects of minor Zr and Er on microstructure and mechanical properties of pure aluminum [J]. Materials Science and Engineering A, 2013, 580: 92−98.

[5] WANG Tong-min, CHEN Zong-ning, FU Hong-wang, GAO Lei, LI Ting-ju. Grain refinement mechanism of pure aluminum by inoculation with Al−B master alloys [J]. Materials Science and Engineering A, 2012, 549: 136−143.

[6] ALI Yahia, QIU Dong, JIANG Bin, PAN Fu-sheng, ZHANG Ming-xing. Current research progress in grain refinement of cast magnesium alloys: A review article [J]. Journal of Alloys and Compounds, 2015, 619: 639−651.

[7] TAMIRISAKANDALA S, BHAT R B, TILEY J S, MIRACLE D B. Grain refinement of cast titanium alloys via trace boron addition [J]. Scripta Materialia, 2005, 53(12): 1421−1426.

[8] HAN Yan-feng, LI Ke, WANG Jun, SHU Da, SUN Bao-de. Influence of high-intensity ultrasound on grain refining performance of Al−5Ti−1B master alloy on aluminium [J]. Materials Science and Engineering A, 2005, 405(1−2): 306−312.

[9] LIMMANEEVICHITR C, EIDHED W. Novel technique for grain refinement in aluminum casting by Al−Ti−B powder injection [J]. Materials Science and Engineering A, 2003, 355(1−2): 174−179.

[10] LU L, DAHLE A K. Effects of combined additions of Sr and AlTiB grain refiners in hypoeutectic Al−Si foundry alloys [J]. Materials Science and Engineering A, 2006, 435−436: 288−296.

[11] WANNASIN J, CANYOOK R, WISUTMETHANGOON S, FLEMINGS M C. Grain refinement behavior of an aluminum alloy by inoculation and dynamic nucleation [J]. Acta Materialia, 2013, 61(10): 3897−3903.

[12] WANNASIN J, MARTINEZ R A, FLEMINGS M C. Grain refinement of an aluminum alloy by introducing gas bubbles during solidification [J]. Scripta Materialia, 2006, 55(2): 115−118.

[13] CHEN Hang, JIE Jin-chuan, FU Ying, MA Hong-jun, LI Ting-ju. Grain refinement of pure aluminum by direct current pulsed magnetic field and inoculation [J]. Transactions of Nonferrous Metals Society of China, 2014, 24(5): 1295−1300.

[14] VASHEGHANI F M, EMADODDIN E, EMAMY M, HONARBAKHSH R A. Effect of grain refinement on mechanical properties and sliding wear resistance of extruded Sc-free 7042 aluminum alloy [J]. Materials & Design, 2014, 54: 361−367.

[15] LÜ Xin-yu, GUO Er-jun, ROMETSCH P, WANG Li-juan. Effect of one-step and two-step homogenization treatments on distribution of Al_3Zr dispersoids in commercial AA7150 aluminium alloy [J]. Transactions of Nonferrous Metals Society of China, 2012, 22(11): 2645−2651.

[16] TANG Chao-lan, ZHOU De-jing. Precipitation hardening behavior of dilute binary Al−Yb alloy [J]. Transactions of Nonferrous Metals Society of China, 2014, 24(7): 2326−2330.

[17] DUAN Y L, XU G F, PENG X Y, DENG Y, LI Z, YIN Z M. Effect of Sc and Zr additions on grain stability and superplasticity of the simple thermal-mechanical processed Al−Zn−Mg alloy sheet [J]. Materials Science and Engineering A, 2015, 648: 80−91.

[18] EASTON M A, STJOHN D H. A model of grain refinement incorporating alloy constitution and potency of heterogeneous nucleant particles [J]. Acta Materialia, 2001, 49(10): 1867−1878.

[19] STJOHN D H, QIAN M, EASTON M A, CAO P, HILDEBRAND Z. Grain refinement of magnesium alloys [J]. Metallurgical and Materials Transactions A, 2005, 36(7): 1669−1679.

[20] GREER A L, BUNN A M, TRONCHE A, EVANS P V, BRISTOW D J. Modelling of inoculation of metallic melts: Application to grain refinement of aluminium by Al−Ti−B [J]. Acta Materialia, 2000, 48(11): 2823−2835.

[21] WANG Feng, QIU Dong, LIU Zhi-lin, TAYLOR J A, EASTON M A, ZHANG Ming-xing. Crystallographic study of Al_3Zr and Al_3Nb as grain refiners for Al alloys [J]. Transactions of Nonferrous Metals Society of China, 2014, 24(7): 2034−2040.

[22] WANG Feng, QIU Dong, LIU Zhi-lin, TAYLOR J A, EASTON M A, ZHANG Ming-xing. Crystallographic study of grain refinement of Al by Nb addition [J]. Journal of Applied Crystallography, 2014, 47(2): 770−779.

[23] JIANG Bin, LIU Wen-jun, QIU Dong, ZHANG Ming-xing, PAN Fu-sheng. Grain refinement of Ca addition in a twin-roll-cast Mg−3Al−1Zn alloy [J]. Materials Chemistry and Physics, 2012, 133(2-3): 611−616.

[24] WANG Feng, QIU Dong, LIU Zhi-lin, TAYLOR J A, EASTON M A, ZHANG Ming-xing. The grain refinement mechanism of cast

aluminium by zirconium [J]. Acta Materialia, 2013, 61(15): 5636−5645.
[25] EASTON M, STJOHN D. Grain refinement of aluminum alloys: Part I. The nucleant and solute paradigms-a review of the literature [J]. Metallurgical and Materials Transactions A, 1999, 30(6): 1613−1623.
[26] EASTON M, STJOHN D. Grain refinement of aluminum alloys: Part II. Confirmation of, and a mechanism for, the solute paradigm [J]. Metallurgical and Materials Transactions A, 1999, 30(6): 1625−1633.
[27] JOHNSSON M, BACKERUD L, SIGWORTH G K. Study of the mechanism of grain refinement of aluminum after additions of Ti- and B-containing master alloys [J]. Metallurgical Transactions A, 1993, 24(2): 481−491.
[28] STJOHN D H, QIAN M, EASTON M A, CAO P. The interdependence theory: The relationship between grain formation and nucleant selection [J]. Acta Materialia, 2011, 59(12): 4907−4921.
[29] WU H, WEN S P, GAO K Y, HUANG H, WANG W, NIE Z R. Effect of Er additions on the precipitation strengthening of Al−Hf alloys [J]. Scripta Materialia, 2014, 87: 5−8.
[30] CHEN Zhong-wei, HE Zhi, JIE Wan-qi. Growth restriction effects during solidification of aluminium alloys [J]. Transactions of Nonferrous Metals Society of China, 2009, 19(2): 410−413.
[31] WANG Feng, LIU Zhi-lin, QIU Dong, TAYLOR J A, EASTON M A, ZHANG Ming-xing. The influence of the effect of solute on the thermodynamic driving force on grain refinement of Al alloys [J]. Metallurgical and Materials Transactions A, 2015, 46(1): 505−515.
[32] EASTON M, STJOHN D. An analysis of the relationship between grain size, solute content, and the potency and number density of nucleant particles [J]. Metallurgical and Materials Transactions A, 2005, 36(7): 1911−1920.
[33] BOLZONI L, NOWAK M, HARI BABU N. Grain refining potency of Nb−B inoculation on Al−12Si−0.6Fe−0.5Mn alloy [J]. Journal of Alloys and Compounds, 2015, 623: 79−82.
[34] EASTON M, DAVIDSON C, STJOHN D. Grain morphology of as-cast wrought aluminium alloys [J]. Materials Transactions, 2011, 52(5SI): 842−847.
[35] WANG Feng, LIU Zhi-lin, QIU Dong, TAYLOR J A, EASTON M A, ZHANG Ming-xing. Revisiting the role of peritectics in grain refinement of Al alloys [J]. Acta Materialia, 2013, 61(1): 360−370.
[36] BERMINGHAM M J, MCDONALD S D, DARGUSCH M S, STJOHN D H. The mechanism of grain refinement of titanium by silicon [J]. Scripta Materialia, 2008, 58(12): 1050−1053.
[37] ROKHLIN L L, BOCHVAR N R, DOBATKINA T V, EV V G L. Al-rich portion of the Al−Hf phase diagram [J]. Russian Metallurgy (Metally), 2009, 2009(3): 258−262.
[38] JIA Zhi-hong, HUANG Hui-lan, WANG Xue-li, XING Yuan, LIU Qing. Hafnium in aluminum alloys: A review [J]. Acta Metallurgica Sinica (English Letters), 2016, 29(2): 105−119.
[39] LEE S, UTSUNOMIYA A, AKAMATSU H, NEISHI K, FURUKAWA M, HORITA Z, LANGDON T G. Influence of scandium and zirconium on grain stability and superplastic ductilities in ultrafine-grained Al−Mg alloys [J]. Acta Materialia, 2002, 50(3): 553−564.
[40] LI J H, WIESSNER M, ALBU M, WURSTER S, SARTORY B, HOFER F, SCHUMACHER P. Correlative characterization of primary Al_3(Sc,Zr) phase in an Al−Zn−Mg based alloy [J]. Materials Characterization, 2015, 102: 62−70.

铪元素对铸造铝合金晶粒细化的机制

李红英[1]，李德望[1]，祝志祥[2,3]，陈保安[2,3]，陈 新[2,3]，杨长龙[4]，张宏宇[4]，康 巍[1]

1. 中南大学 材料科学与工程学院，长沙 410083；
2. 全球能源互联网研究院 电工新材料与微电子研究所，北京 102211；
3. 先进输电技术国家重点实验室，北京 102211；
4. 国网辽宁省电力有限公司，沈阳 110006

摘 要：通过金相显微镜观察、电子显微观察和 X 射线衍射分析研究了铪元素的加入对铸造铝合金晶粒细化的影响。研究结果表明，铪元素的加入可以有效地细化合金晶粒，在凝固过程中铪元素可与铝反应形成 Al_3Hf 粒子，初生的 Al_3Hf 粒子可以作为基体有效的形核质点，与基体共格、纳米级别的 Al_3Hf 粒子可以通过钉扎效应抑制晶粒的长大。由溶质原子理论和晶体学研究确定了实验合金的晶粒细化机制，具有两种不同的类型：低铪含量的细化效应主要是由 Hf 原子引发的成分过冷所致，中铪和高铪含量的细化效应为溶质原子与 Al_3Hf 粒子共同作用所致。

关键词：晶粒细化机制；铝合金；铸造；铪；Al_3Hf

(Edited by Yun-bin HE)